

Machine-learning correction for the calorimeter saturation of cosmic-rays ions with the Dark Matter Particle Explorer: towards the PeV scale

Andrea Serpolla^{1,*}, Andrii Tykhonov¹, Paul Coppin¹, Manbing Li¹, Andrii Kotenko¹, Enzo Putti-Garcia¹, Hugo Boutin¹, Mikhail Stolpovskiy³, Jennifer Maria Frieden², Chiara Perrina², Xin Wu¹

¹*Département de physique nucléaire et corpusculaire (DPNC), Université de Genève (UniGE), Quai Ernest-Ansermet 24, Geneva, CH-1205, Switzerland*

²*Institute of Physics, Ecole Polytechnique Fédérale de Lausanne (EPFL), Lausanne, CH-1015, Switzerland*

³*International Space Science Institute (ISSI), Hallerstrasse 6, Bern, CH-3012, Switzerland*

Abstract

The Dark MATter Particle Explorer (DAMPE) instrument is a space-born cosmic-ray detector, capable of measuring ion fluxes up to ~ 500 TeV/n. This energy scale is made accessible through its calorimeter, which is the deepest currently operating in orbit. Saturation of the calorimeter readout channels start occurring above ~ 100 TeV of incident energy, and can significantly affect the primary energy reconstruction. Different techniques, analytical and machine-learning based, have been developed to tackle this issue, focusing on the recovery of single-bar deposits, up to several hundreds of TeV. In this work, a new machine-learning technique is presented, which profit of a unique model to correct the total deposited energy in DAMPE calorimeter. The described method is able to generalise its corrections for different ions and extend the maximum detectable incident energy to the PeV scale.

Keywords: calorimeters, cosmic rays, machine learning, energy reconstruction, DAMPE

1. Introduction

Galactic cosmic rays (GCRs) are accelerated high-energy particles wandering in our galaxy. Their origin and interaction with the interstellar medium (ISM) are crucial topics in astrophysics [1]. One of the main challenges in GCR studies is the accurate measurement of their composition and energy, which are essential to probe their generation in our galaxy and propagation in the ISM. More specifically, a key open question is the behaviour of heavy nuclei fluxes at the 100 TeV to PeV scale; this work is a necessary and important step to achieve such goal.

The DArk Matter Particle Explorer (DAMPE) is a space-based detector operating since its launch in December 2015 [2]. DAMPE is capable of detecting CR nuclei, electrons/positrons and γ -rays, thanks to its four sub-detectors: a plastic scintillator (PSD) [3], a silicon-tungsten tracker-converter (STK) [4], a bismuth germanium oxide (BGO) electromagnetic calorimeter [5], and a neutron detector (NUD) [6]. The DAMPE instrument allows to detect and study γ -rays and electrons/positrons from ~ 5 GeV up to several TeVs [7, 8], and CR nuclei from ~ 50 GeV up to several hundreds of TeVs [9–11]. DAMPE stands out over other space-based instruments because of its calorimeter, the deepest currently in orbit with its 32 radiation lengths, or 1.6 nuclear interaction lengths. Above ~ 100 TeV

of kinetic energy, the most readout channels can saturate; in this case, a significant part of information about the deposited particle energy gets lost, making the incident energy reconstruction more problematic. Saturation is particularly relevant for heavy nuclei—such as iron, which can release a significant amount of energy in a single channel.

Previous studies have shown the possibility of recovering the lost energy due to saturation using analytical [12], or machine-learning (ML) techniques [13]. However, these methods start losing accuracy and precision for heavy nuclei, and for incident energies above ~ 500 TeV. Therefore, the development of techniques that can help correcting for saturation at higher energies and for heavy nuclei is crucial for the measurement of GCRs spectra beyond the multi-TeV scale. In this work, we present a ML method to correct the total deposited energy in DAMPE calorimeter for saturation up to few PeVs of primary energy, that can be applied to light ions (e.g., protons, helium) as well as on heavier ones (e.g., carbon, oxygen, iron).

2. The BGO calorimeter of DAMPE

Figure 1 shows a view of the DAMPE calorimeter, with its 14 layers and 22 BGO bars per layer [2, 14]. The bars have dimensions of $2.5 \times 2.5 \times 60$ cm³ and are alternately arranged along the x - and y - directions, resulting in a total active area on the vertical axis of 60×60 cm². The energy releases in the bars are measured through scintillation, by photomultiplier tubes (PMTs) coupled to both ends of a

*Corresponding author

Email address: andrea.serpolla@cern.ch (Andrea Serpolla)

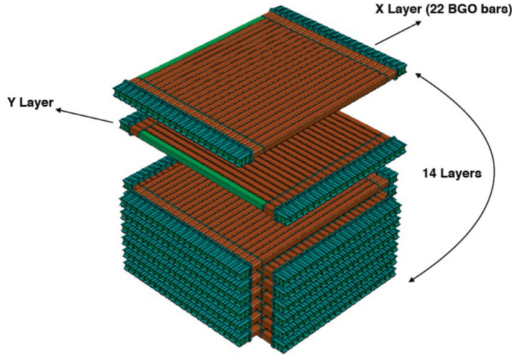


Figure 1: schematic view of the DAMPE calorimeter [2].

bar—namely S0 and S1, using optical fibers. The attenuation at the S1 end is five times higher than the one at S0, making S1 more suitable to measure higher deposits. The PMTs used in DAMPE calorimeter are the R5610A-01 type, produced by Hamamatsu, and they provide 10 different stages of charge amplification, or dynodes, identified as Dy1–10 [15]. For the offline analysis, only signals from three of the available dynodes are recorded, specifically the ones from Dy2, Dy5 and Dy8. The three channels have different gain factors, achieving a dynamic and wider range of measurable energies. Dynode Dy8 has the highest gain, and therefore is the most sensitive to low signals; Dy2 has the lowest gain, and is the most proper to measure high energy depositions. The Dy8 channels cover the range 2–500 MeV at the S0 end, and 10 MeV–2.5 GeV at S1; Dy5, 80 MeV–20 GeV at S0, and 400 MeV–100 GeV at S1; Dy2, 3.2 GeV–800 GeV at S0, and 16 GeV–4 TeV at S1 [2]. When a read signal exceeds the maximum measurable value of the low-gain channel (i.e., Dy2) at the S1 end, the reading is discarded. In this situation, the bar is considered saturated and the energy deposited in that bar will be null. For an example of a saturated event, see Figure 2.

3. Method

The energy lost due to saturation in a calorimeter can be recovered using several methods and approaches. Previous works have shown the feasibility of performing such task using analytical and machine-learning methods [12, 13]. Although their success in recovering the energy lost in saturation, previously published methods need specific corrections for different ions and start losing accuracy above ~ 500 TeV. In this work, a new ML model to correct the total deposited energy in a calorimeter is presented. The new model provides a correction that is independent from the type of ion crossing the detector and maintains its accuracy up to few PeVs of incident energy. These two features are fundamental for the analyses of the individual CR fluxes, as well as the all-particle spectrum, and the probing of the knee region, where a change of the spectral

index is expected. To train the model and validate the final correction, different ions crossing the full DAMPE experiment are simulated.

3.1. Event simulation and selection

Ions crossing the DAMPE instrument are simulated with the version 10.5 of the GEANT4 toolkit [16], using the FTFP_BERT physics list [17]; for primary energies above 100 TeV, the EPOS-LHC hadronic physics model is used interfaced to GEANT4 through the Cosmic Ray Monte Carlo (CRMC) package [18–20].

Using the calorimeter hits, χ^2 fits are independently performed in the xz - and yz - views to determine the particle trajectories. To ensure a proper containment in DAMPE calorimeter, and exclude non-reliable χ^2 fits, a series of preliminary selections is applied to the simulated events; in particular:

- no single layer should contain alone more than 35% of the total energy;
- the maximum deposit for the three layers after the first one should not belong to the edge bars;
- the extrapolated positions of the reconstructed shower vector at the top and at the bottom of the calorimeter active volume should be within 280 mm from the volume center along the x - and y - directions.

This requirements are also in most cases applied to on-orbit data during flux measurements. An additional condition required to improve the quality of the simulated samples, is that the true track is fully contained in the active volume of the calorimeter. For the model training, events with a deposited energy inferior than 1 TeV are not considered; this condition is removed for the final results.

3.2. Identification of events with saturation

An algorithm to identify saturated bars is developed to later select events with saturation. Simply considering bars with null deposits as saturated is not enough, because it does not discriminate the case where the ion does not cross the bar at all. Saturation occurs in the middle of the shower profile, where the deposit is at its maximum. According to this feature, the information of adjacent bars can be used to assess if a null deposit is real or caused by saturation. In this work, a bar is considered saturated when either the left or right neighbour on the same layer has a deposit greater than 25 GeV. In a recurrent fashion, a bar is identified as saturated also when its deposit is null and a neighbour is saturated according to the previous condition; this is iterated until a non-null deposit or the edge of the layer is found.

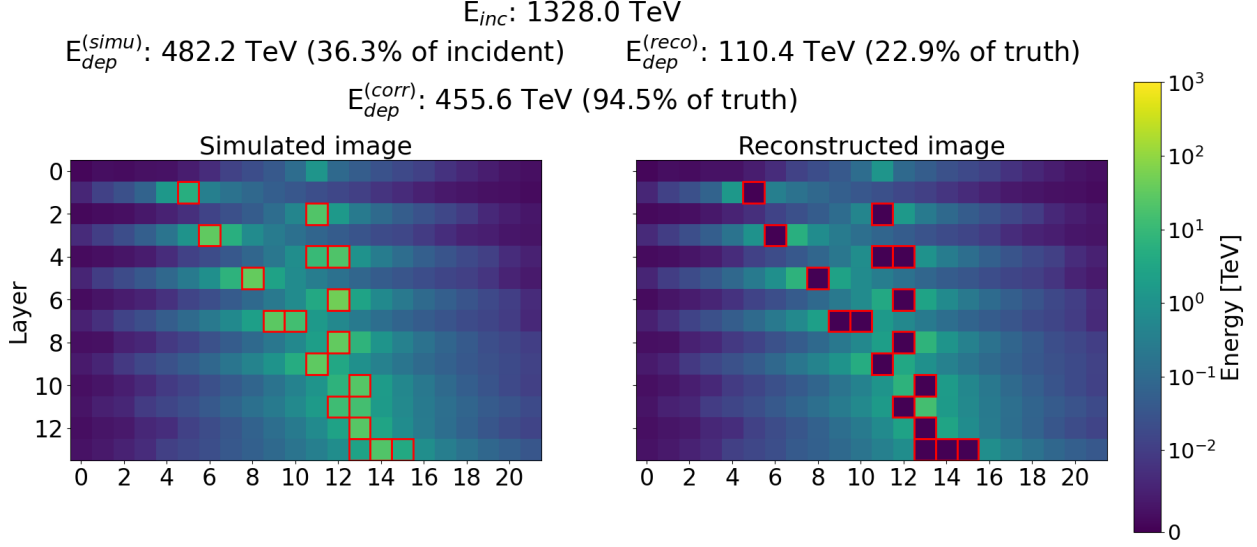


Figure 2: simulated event of an iron nucleus crossing the DAMPE calorimeter, with an incident energy of ~ 1.3 PeV. The figure shows the simulated (on the left) and the reconstructed energy deposits (on the right) on the single BGO bars. Each subplot merges the information from both the layers with x- (odd layers) and y-oriented (even layers) bars. In the reconstructed event, null deposits resulting from saturation are present in the middle of the shower axis, where the release of energy is at its maximum. In both plots, the saturated bars are highlighted with red boxes. In the shown event, $\sim 80\%$ of the true deposited energy is lost because of saturation; after correction, more than 90% of the true deposit is recovered.

3.3. Model architecture

Convolutional neural networks (CNNs) are typically used in ML applications for images processing [21]. A picture of width W and height H can be given as input to these models as an array of shape $W \times H$. Similarly, the bar deposits of DAMPE calorimeter can be treated as a one-channel image of shape 14×22 ; the plots of Figure 2 give a visual representation of this. Following this premise, a CNN can be designed to provide a correction factor for the total deposited energy, in the presence of saturation; this approach has been already proved successful in [13]. Figure 3 shows the architecture selected in this work. The developed model can be divided into two main sections: first, a series of convolutional layers extracts features from the input image; then, the resulting output is flattened, and passed to a second series of dense layers, that provide the final correction factor in output. To implement the ML architecture, TensorFlow 2.1.0 is used in this work [22]. The used architecture follows the same structure of the model shown in Figure 4 of [23], with the only differences that the two input variables for the total deposited energy and the maximum bar deposit—i.e., $E_{BGO \text{ Total}}$ and $E_{BGO \text{ barmax}}$ in the Figure, have been removed and that one value is returned as output, instead of four.

3.4. Model training

To generalise the correction for different ions, a model has been trained using simulations of protons, helium, lithium, beryllium, boron, carbon, nitrogen, oxygen, neon, magnesium, silicon and iron nuclei. Protons, helium, carbon, oxygen and silicon events range between 100 TeV and

1 PeV, iron between 100 TeV and 3 PeV, and the remaining elements between 100 TeV and 500 TeV. The model is provided with all the events, without specifically selecting saturated events, so that it can also learn when no correction is needed.

ML models generally perform better when given input values belonging to the same range. Several normalisations can be applied to the inputs for this purpose; for this work, the model is trained on BGO images previously divided by their maximum bar deposit. In the same perspective, the CNN is trained to predict the target value

$$\lambda = \ln \left(\frac{E_{dep}^{(simu)}}{E_{dep}^{(reco)}} \right), \quad (1)$$

with $E_{dep}^{(simu)}$, $E_{dep}^{(reco)}$ respectively the simulated and reconstructed total deposited energy in the calorimeter.

The full dataset contains a total of 2.13 million events, which are split into training (1.92 million events, i.e., 90% of the full dataset) and validation sample (0.21 million events, i.e., 10% of the full dataset). The validation sample is needed to verify the model is not over-trained. When that happens, the model loss evaluated on the validating events starts increasing, despite the training loss keeps decreasing. In over-training, the model starts over-fitting the given training events, loosing in generalisation when applied to a different subset of events of the same kind. Figure 4 shows the model loss evaluated on both the training and validation samples. The loss is shown in function of the training epochs, i.e., an iteration over the full set of training events. The model training is stopped at the

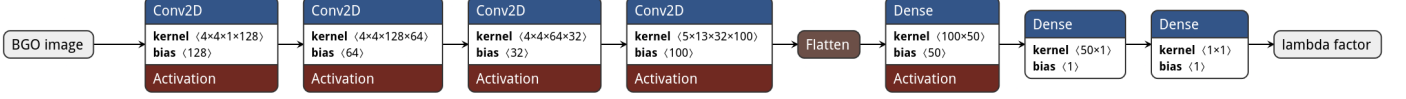


Figure 3: design of a convolutional neural network (CNN) to correct the total deposited energy of the calorimeter image for saturation. The specific model takes as input a $14 \times 22 \times 1$ image, where each pixel corresponds to a bar in the BGO calorimeter, and returns a correction factor for the total energy.

point where the loss function does not further decrease. At most, 50 epochs are needed for the model to converge.

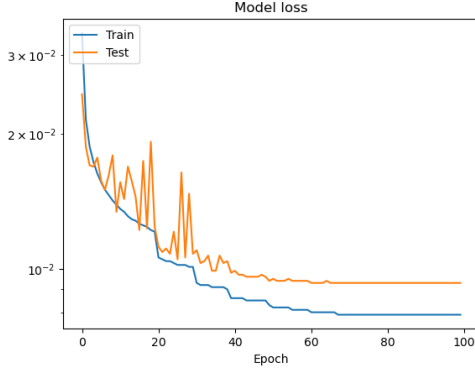


Figure 4: model loss of the trained model. The loss function is evaluated at the end of each training epoch on both the training and the testing sub-samples. The decreasing trend found in both cases, excludes the occurrence of over-training.

4. Results

Simulations of protons, carbon and iron nuclei with primary energies between 100 TeV–1 PeV crossing the DAMPE calorimeter are used to validate the trained model. Figure B.10 shows the fraction of saturated events present in the used samples. Figures 5–7 show the ratio of the total reconstructed energy after correction and the corresponding true simulated value, in function of incident energy, fraction of energy lost in saturation and number of saturated bars. Referring to Figures 5 and 7, the primary energy and the number of saturated bars does not seem to substantially affect the accuracy of the correction. On the contrary, Figure 6 shows how the fraction of missing energy impacts the predictions. In particular, highly saturated events with more than $\sim 90\%$ of the true total deposit missing show a stronger bias of $\sim -20\text{--}30\%$. In other cases, the remainder of missing energy does not exceed 10% of the true value.

In Figure 8 the events are re-weighted to a $E_{\text{inc}}^{-2.7}$ spectrum, similarly to an actual CR flux—ignoring possible breaks in the spectral index [24] (see Appendix A for further details). The distribution of deposited energy before and after the correction shows the residual bias for very highly saturated events affects the last energy bins.

5. Conclusion and discussion

An ML method has been developed to correct the deposited energies in a calorimeter, in the presence of saturation. The issue at hand provokes the partial loss of the original energy deposits, due to the inability of the readout electronics to process signals above their maximum capacity. The use of a CNN makes it possible to analyse the BGO image with saturation and recover the original total deposited energy.

Prior to this work, two other corrections were developed to tackle the saturation in DAMPE calorimeter. The work in [12] provides an analytical method to infer the energy lost in saturation using the information from the adjacent bars; the main limitation of this approach is the inability of application where several contiguous saturated bars are found. On the other hand, the work in [13] uses an ML technique to achieve a higher precision; however, the final correction needs the training of two separate CNNs to reconstruct the single energy deposits lost in the middle layers and in the last one of the calorimeter. Also, two specialised trainings are performed for protons and helium, and a bias correction is needed for other ions. Overall, both precedent works succeed in their aim, but they require specific tunings for different ions and start losing accuracy above ~ 500 TeV of incident energy, posing issues for the flux measurements at the PeV scale. In this work, the focus has been moved to the prediction of an overall correction factor for the total deposited energy, instead of reconstructing the single pixels of the BGO image. This novel approach facilitates the model learning, achieving an improved precision. In addition, the introduction of different ion species and higher incident energies in the model training results in an improved accuracy, up to several PeVs. Both the improvements in maximum energy and generalisation supersede previous techniques, and can significantly help in probing the flux of CR ions at the PeV scale, where the knee region—i.e. a change in the all-particle spectral index, is expected to be. On the other hand, highly saturated events with more than 90% of the original deposit lost still require a deeper understanding to eliminate the residual bias.

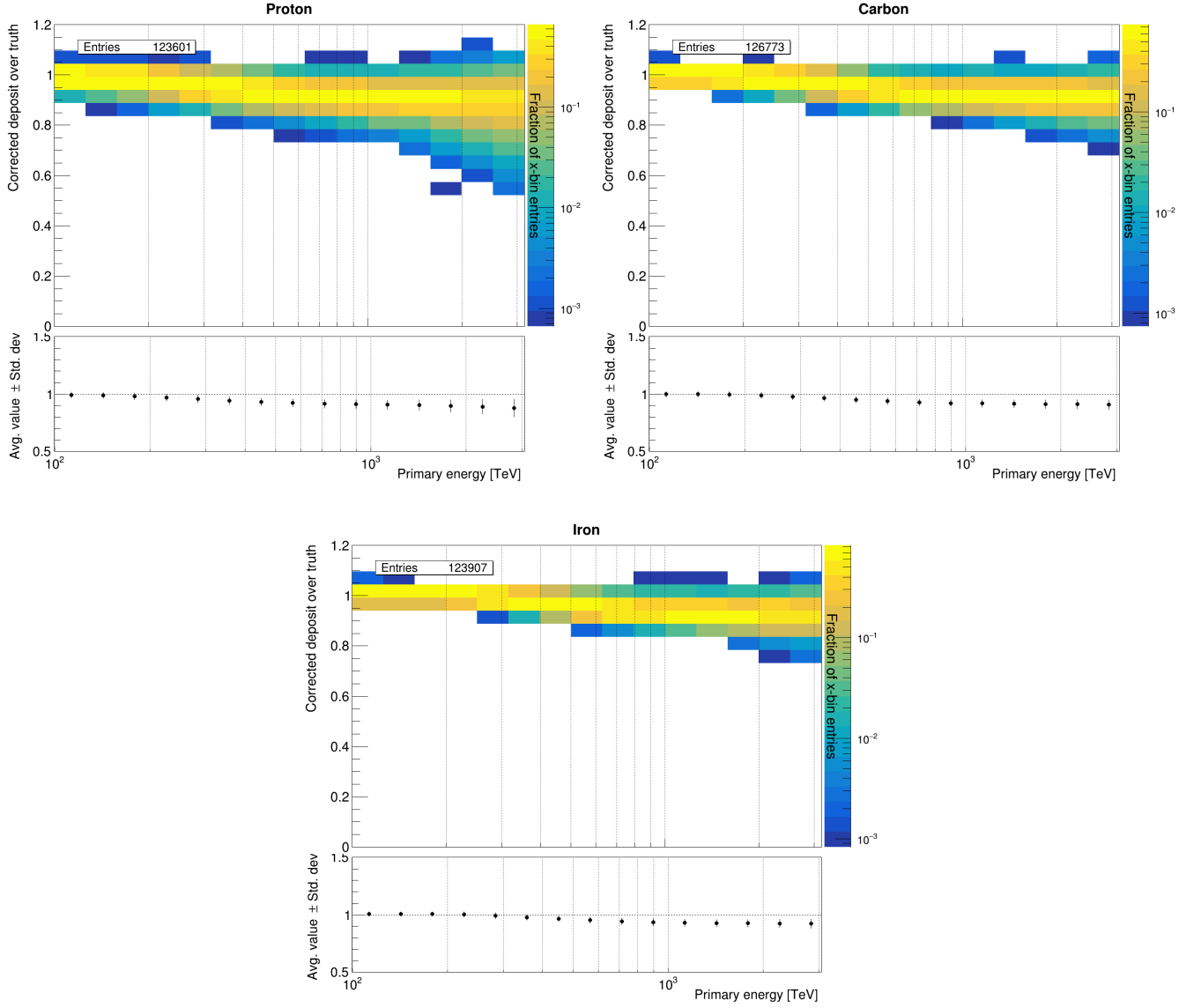


Figure 5: ratio of the corrected and simulated values of the total deposited energy, in function of the particle incident energy. Three plots are shown for the protons (top left), carbon (top right) and iron events (bottom); each plot is split into two subplots: the main one shows the 2D distribution of the events with saturation, while the secondary one shows the average value and standard deviation of the y-projection of the corresponding x-bin.

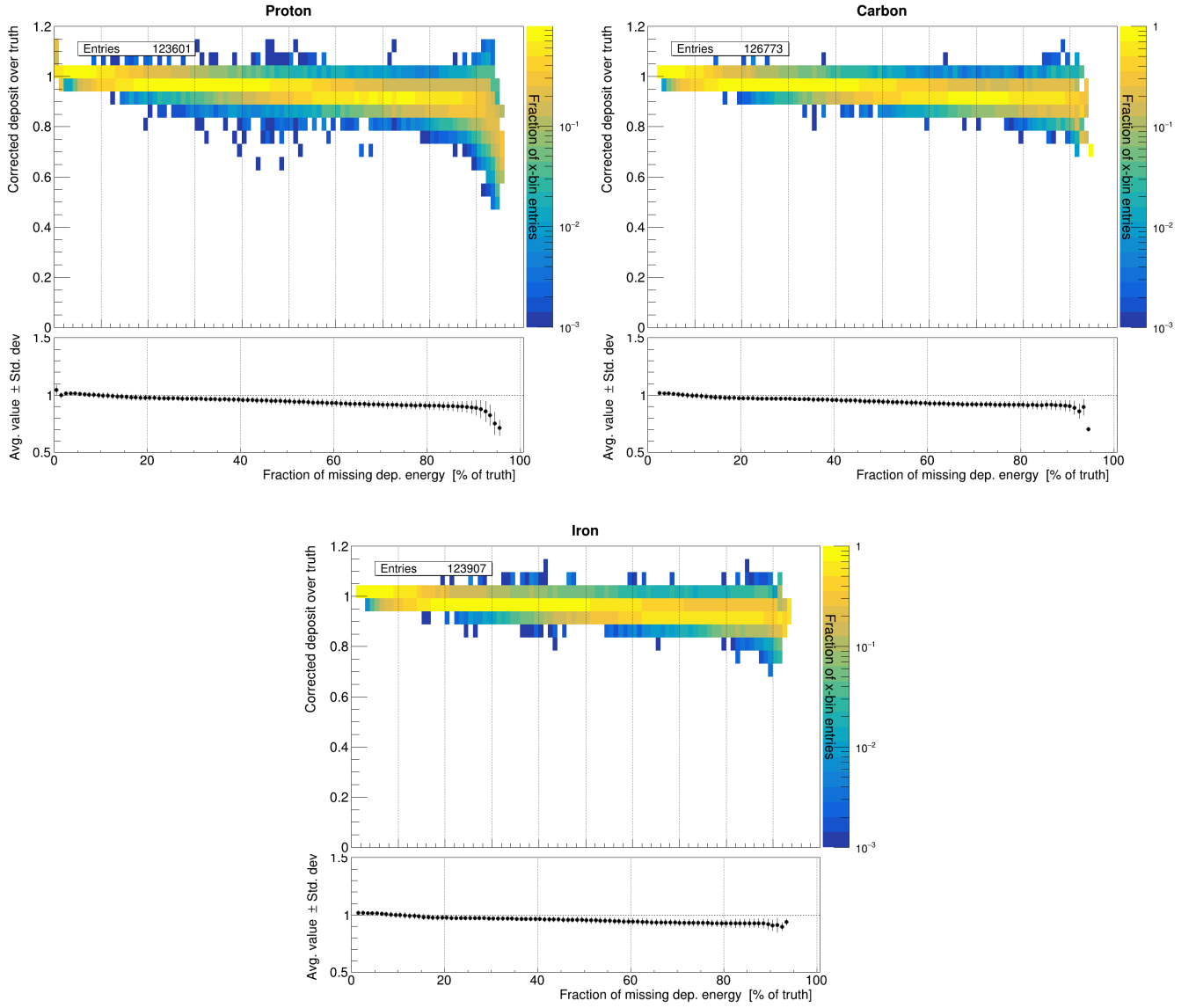


Figure 6: as per Figure 5, but in function of the fraction of true energy lost in saturation.

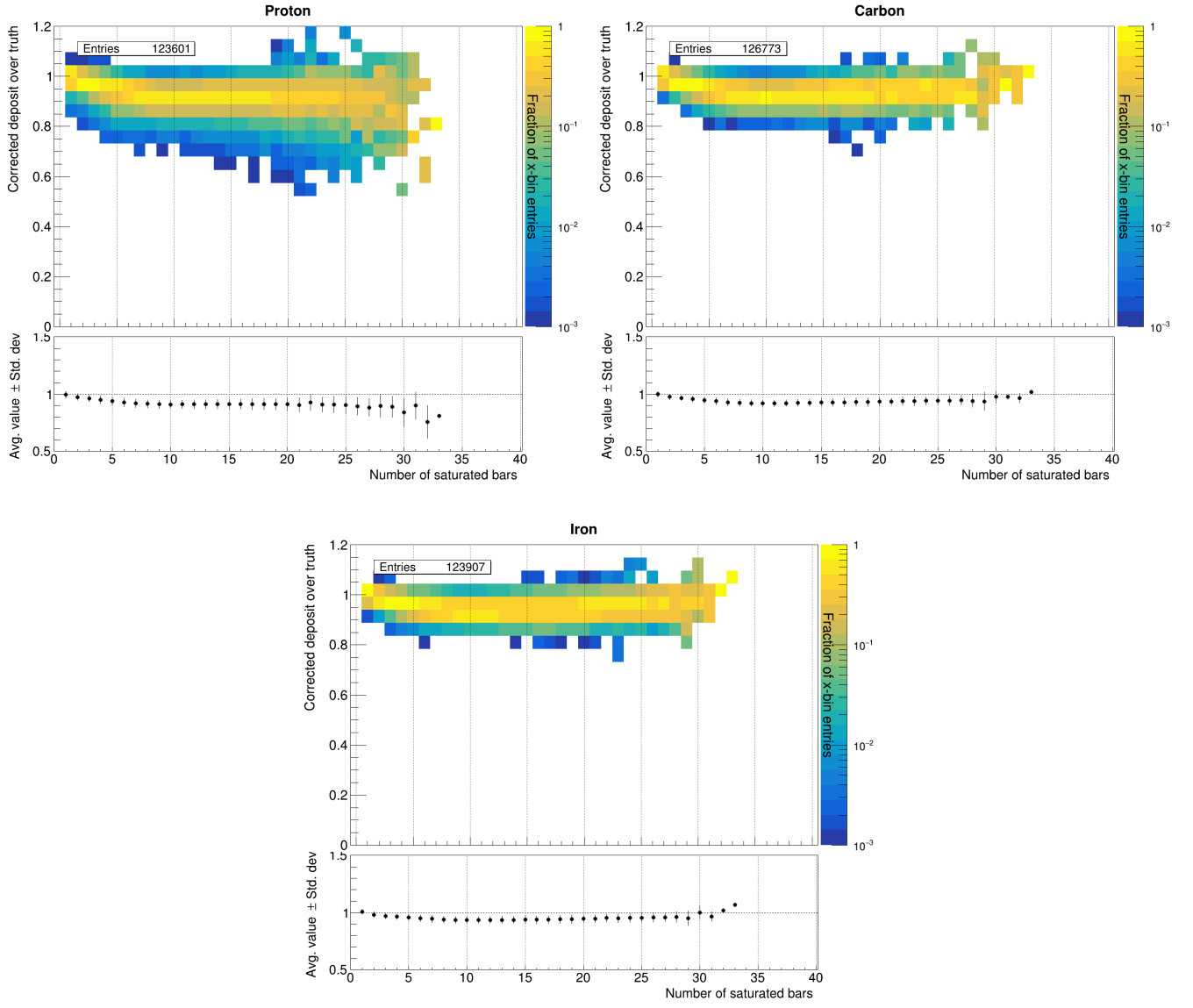


Figure 7: as per Figure 5, but in function of the number of saturated bars.

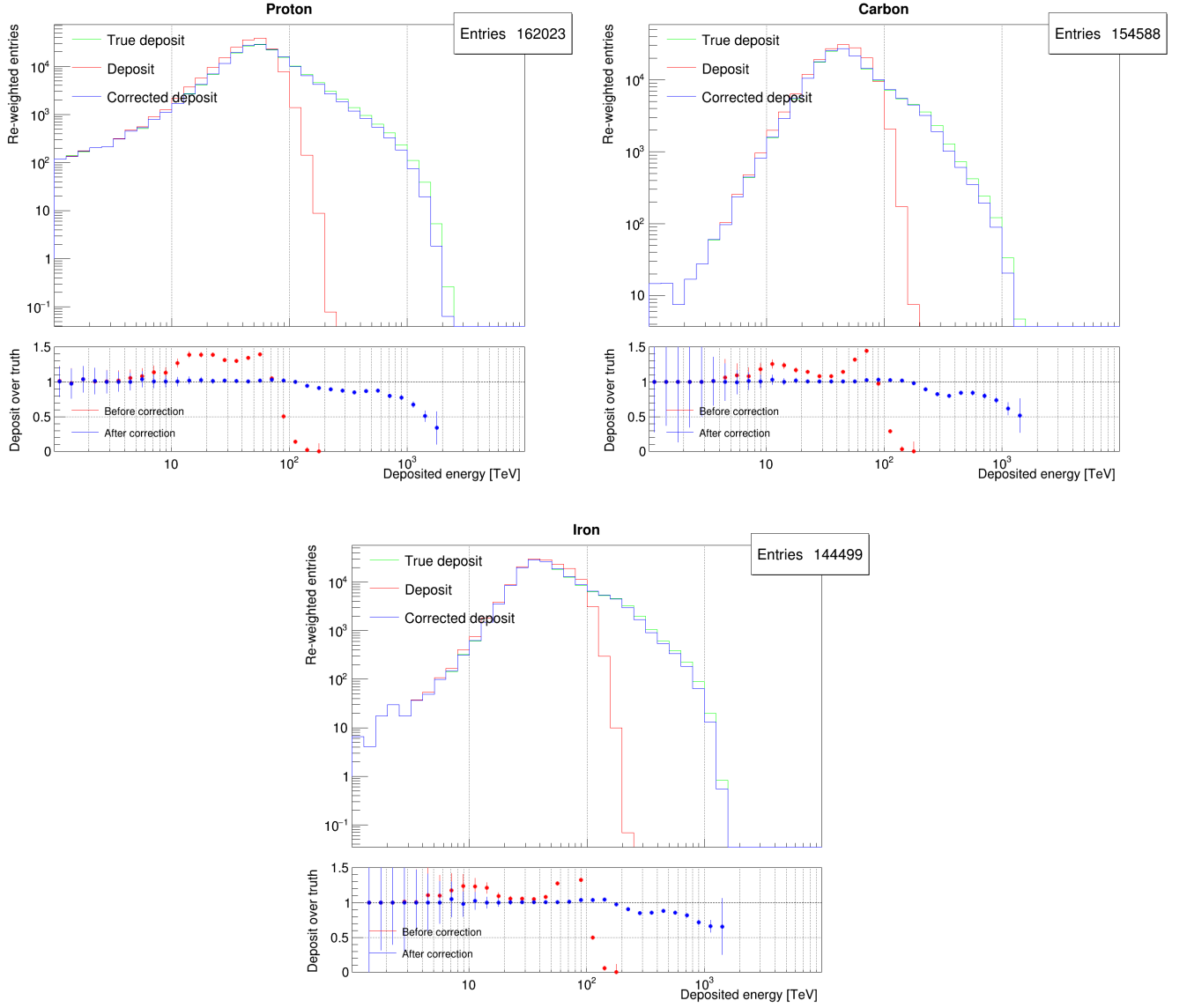


Figure 8: distribution of the total deposited energy of simulated events re-weighted to a $E_{\text{inc}}^{-2.7}$ spectrum, based on their incident energy. Three plots are shown for the protons (top left), carbon (top right) and iron events (bottom); each plot is split into two subplots: the top one shows the distributions of the true value of the total deposited energy, as from simulation (green), and the reconstructed deposit before (red) and after (blue) correction; the bottom one shows the ratio between the bin counts of the reconstructed and simulated energy, before (red) and after (blue) correction.

Appendix A. Events re-weighting

MC simulations generate events with a spectrum $\propto E_{\text{inc}}^{-1}$, with E_{inc} being the incident energy of the generated particle. The used spectral index is not compatible with the observations, that are more compatible with a spectrum $\propto E_{\text{inc}}^{-2.7}$. To re-weight the events to a new spectral index γ , the following weights can be applied:

$$w = \frac{E_{\text{inc}}^{(1-\gamma)}}{N_{\text{tot}} M_{\text{samples}}} , \quad (\text{A.1})$$

with N_{tot} the total number of events and M_{samples} the number of samples covering energy ranges which E_{inc} belongs to. Figure A.9 shows the distributions of proton, carbon and iron events used in this work before and after re-weighting to a $E^{-2.7}$ spectrum.

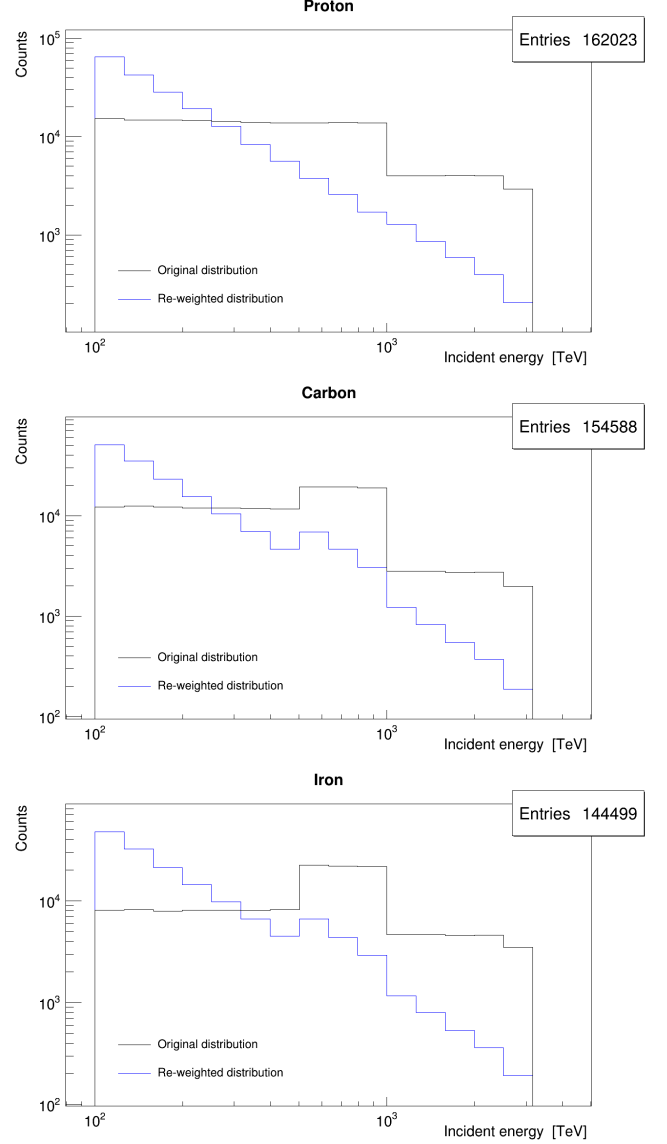


Figure A.9: distribution of the primary energy, before and after re-weighting the entries to a simil-CR spectrum. The events are re-weighted so that the flux $\Phi \propto E_{\text{inc}}^{-2.7}$, with E_{inc} being the incident energy. Three plots are shown here for the protons (top left), carbon (top right) and iron events (bottom). The distributions consider the full simulated samples, after event selection.

Appendix B. Fraction of saturated events

Generally, BGO bars of DAMPE calorimeter are more subject to saturation as the incident energy increases. Figure B.10 shows the fraction of saturated events found in MC simulations of protons, carbon and iron, in function of the incident energy.

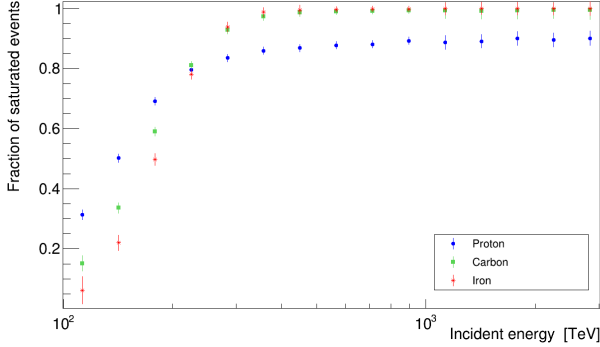


Figure B.10: Fraction of saturated events found in the MC simulations of protons, carbon and iron nuclei crossing DAMPE instrument. The fraction is plotted in function of the true incident energy, and in Figure A.9 it is possible to see the original event distributions with the total counts.

References

- [1] R. Aloisio, P. Blasi, I. De Mitri, et al., Selected Topics in Cosmic Ray Physics, in: Multiple Messengers and Challenges in Astroparticle Physics, Springer International Publishing, 2018, pp. 1–95. [doi:10.1007/978-3-319-65425-6_1](#).
- [2] J. Chang, G. Ambrosi, Q. An, et al., The Dark Matter Particle Explorer mission, *Astroparticle Physics* 95 (2017) 6–24. [doi:10.1016/j.astropartphys.2017.08.005](#).
- [3] Y. Yu, Z. Sun, H. Su, et al., The plastic scintillator detector for DAMPE, *Astroparticle Physics* 94 (2017) 1–10. [doi:10.1016/j.astropartphys.2017.06.004](#).
- [4] P. Azzarello, G. Ambrosi, R. Asfandiyarov, et al., The DAMPE silicon-tungsten tracker, *Nuclear Instruments and Methods in Physics Research Section A: Accelerators, Spectrometers, Detectors and Associated Equipment* 831 (2016) 378–384. [doi:10.1016/j.nima.2016.02.077](#).
- [5] Z. Zhang, Y. Zhang, J. Dong, et al., Design of a high dynamic range photomultiplier base board for the BGO ECAL of DAMPE, *Nuclear Instruments and Methods in Physics Research Section A: Accelerators, Spectrometers, Detectors and Associated Equipment* 780 (2015) 21–26. [doi:10.1016/j.nima.2015.01.036](#).
- [6] M. He, T. Ma, J. Chang, et al., GEANT4 Simulation of Neutron Detector for DAMPE, *Acta Astronomica Sinica* 57 (2016) 1–8.
- [7] F. Alemanno, Q. An, P. Azzarello, et al., Search for gamma-ray spectral lines with the dark matter particle explorer, *Science Bulletin* 67 (7) (2022) 679–684. [doi:10.1016/j.scib.2021.12.015](#).
- [8] G. Ambrosi, Q. An, R. Asfandiyarov, et al., Direct detection of a break in the teraelectronvolt cosmic-ray spectrum of electrons and positrons, *Nature* 552 (7683) (2017) 63–66. [doi:10.1038/nature24475](#).
- [9] F. Alemanno, C. Altomare, Q. An, et al., Measurement of the cosmic $p + \text{He}$ energy spectrum from 50 gev to 0.5 pev with the dampe space mission, *Phys. Rev. D* 109 (2024) L121101. [doi:10.1103/PhysRevD.109.L121101](#).
- [10] F. Alemanno, et al., Observation of a spectral hardening in cosmic ray boron spectrum with the dampe space mission, *Phys. Rev. Lett.* 134 (2025) 191001. [doi:10.1103/PhysRevLett.134.191001](#).
- [11] DAMPE collaboration, Detection of spectral hardenings in cosmic-ray boron-to-carbon and boron-to-oxygen flux ratios with dampe, *Science Bulletin* 67 (21) (2022) 2162–2166. [doi:10.1016/j.scib.2022.10.002](#).
- [12] C. Yue, P. Ma, M. Di Santo, et al., Correction method for the readout saturation of the dampe calorimeter, *Nuclear Instruments and Methods in Physics Research Section A: Accelerators, Spectrometers, Detectors and Associated Equipment* 984 (2020) 164645. [doi:10.1016/j.nima.2020.164645](#).
- [13] M. Stolpovskiy, X. Wu, A. Tykhonov, et al., Machine learning-based method of calorimeter saturation correction for helium flux analysis with dampe experiment, *Journal of Instrumentation* 17 (06) (2022) P06031. [doi:10.1088/1748-0221/17/06/P06031](#).
- [14] Z. Zhang, Y. Zhang, J. Dong, et al., Design of a high dynamic range photomultiplier base board for the bgo ecal of dampe, *Nuclear Instruments and Methods in Physics Research Section A: Accelerators, Spectrometers, Detectors and Associated Equipment* 780 (2015) 21–26. [doi:10.1016/j.nima.2015.01.036](#).
- [15] Photomultiplier tube R5610A | Hamamatsu Photonics. URL https://www.hamamatsu.com/eu/en/product/optical-sensors/pmt/pmt_tube-alone/head-on-type/R5610A.html
- [16] S. Agostinelli, J. Allison, K. Amako, et al., Geant4—a simulation toolkit, *Nuclear Instruments and Methods in Physics Research Section A: Accelerators, Spectrometers, Detectors and Associated Equipment* 506 (3) (2003) 250–303. [doi:10.1016/S0168-9002\(03\)01368-8](#).
- [17] J. Allison, K. Amako, J. Apostolakis, et al., Recent developments in geant4, *Nuclear Instruments and Methods in Physics Research Section A: Accelerators, Spectrometers, Detectors and Associated Equipment* 835 (2016) 186–225. [doi:10.1016/j.nima.2016.06.125](#).
- [18] Air Shower Physics / CRMC · GitLab. URL <https://gitlab.iap.kit.edu/AirShowerPhysics/crmc>
- [19] T. Pierog, I. Karpenko, J. M. Katzy, et al., EPOS LHC: Test of collective hadronization with data measured at the CERN Large Hadron Collider, *Phys. Rev. C* 92 (3) (2015) 034906. [doi:10.1103/PhysRevC.92.034906](#).
- [20] A. Tykhonov, D. Droz, C. Yue, et al., TeV–PeV hadronic simulations with DAMPE, in: Proceedings of 36th International Cosmic Ray Conference — PoS(ICRC2019), Vol. 358, SISSA Medialab, 2021, p. 143. [doi:10.22323/1.358.0143](#).
- [21] A. Ajit, K. Acharya, A. Samanta, A review of convolutional neural networks, in: 2020 International Conference on Emerging Trends in Information Technology and Engineering (ic-ETITE), 2020, pp. 1–5. [doi:10.1109/ic-ETITE47903.2020.049](#).
- [22] M. Abadi, A. Agarwal, P. Barham, et al., TensorFlow: Large-scale machine learning on heterogeneous systems, software available from tensorflow.org (2015). URL <https://www.tensorflow.org/>
- [23] A. Tykhonov, A. Kotenko, P. Coppin, et al., A deep learning method for the trajectory reconstruction of cosmic rays with the dampe mission, *Astroparticle Physics* 146 (2023) 102795. [doi:10.1016/j.astropartphys.2022.102795](#).
- [24] S. Navas, C. Amsler, T. Gutsche, et al., Review of particle physics, *Phys. Rev. D* 110 (2024) 030001. [doi:10.1103/PhysRevD.110.030001](#).